Valence-Detrapping Modes for Electron Transfer in the Solid State of Mixed-Valence, Oxo-Centered, Trinuclear Iron Acetate Complexes: X-ray Structure and Physical Data for $[Fe_3O(O_2CCH_3)_6(4\text{-Et-py})_3](4\text{-Et-py})$

Seung M. Oh,[1] David N. Hendrickson,*[1] Karen L. Hassett,[2] and Raymond E. Davis*[2]

Contribution from the School of Chemical Sciences, University of Illinois, Urbana, Illinois 61801, and the Department of Chemistry, University of Texas, Austin, Texas 78712. *Received June 12, 1985*

Abstract: The rate of *intra*molecular electron transfer in trinuclear, oxo-centered, mixed-valence iron acetates is shown to be affected by the solid-state environment. Lattice dynamics associated with the motion of ligands and/or solvate molecules influence the electron-transfer rate. The X-ray structure of $[Fe_3O(O_2CCH_3)_6(4\text{-Et-py})_3](4\text{-Et-py})$, where 4-Et-py is 4-ethylpyridine, has been determined at 163 and 298 K with use of the heavy-atom method, in conjunction with data measured on a four-circle diffractometer. At 163 K the discrepancy factors are $R = 0.0457$ and $R_w = 0.0425$ for 2847 observed ($F > 6\sigma(F)$) reflections. At 298 K the discrepancy factors are $R = 0.0525$ and $R_w = 0.0546$ for 2809 observed ($F > 6\sigma(F)$) reflections. At both temperatures the compound crystallizes in the monoclinic space group $C2/c$ with four formula weights in a cell which has the following dimensions: at 163 K, $a = 17.060$ (6) Å, $b = 16.943$ (7) Å, $c = 16.183$ (8) Å, and $\beta = 104.49$ (4)°; at 298 K, $a = 17.142$ (3) Å, $b = 17.004$ (1) Å, $c = 16.571$ (4) Å, and $\beta = 104.27$ (2)°. At both temperatures there are two elements of disorder: the 4-Et-py solvate molecule is disordered about a center of inversion and one 4-Et-py ligand is disordered about a C_2 axis which runs through the O^{2-} ion and one iron ion. The dimensions in the mixed-valence Fe_3O complex change appreciably with a change in sample temperature. The Fe_3 triangle becomes more symmetric at the higher temperature. At 163 K the bond distances to the central oxide ion are appreciably different; one iron ion is Fe^{II} and the other two are Fe^{III}. These two Fe–O(oxide) bond distances are closer to being equal in the 298 K structure. It is suggested that a conversion of the unique 4-Et-py ligand from static at low temperatures to dynamic in the solid state at high temperatures is what controls the rate of *intra*molecular electron transfer. Variable-temperature ^{57}Fe Mössbauer data are presented for the series $[Fe_3O(O_2CCH_3)_6(py)_3](solvate)$ to show that the rate of *intra*molecular electron transfer in the mixed-valence complex is dramatically affected by changing the solvate molecule. When there is no solvate molecule present, the complex remains localized on the Mössbauer time scale from 120 to 315 K, whereas the complexes with either pyridine or benzene solvate molecules exhibit temperature-dependent Mössbauer spectra. At low temperatures they show two doublets; at room temperature only a single average doublet is seen. The 4-Et-py compound also shows this same basic type of temperature dependence in its Mössbauer spectrum. In this case the area ratio of "Fe^{III}" to "Fe^{II}" doublets varies from 2:1 below ~100 K to gradually become 3.55:1 at 298 K. The recoilless fraction of the one "Fe^{II}" site is becoming appreciably smaller at high temperatures relative to that for the two "Fe^{III}" sites. This is further evidence for the dynamic nature of the unique 4-Et-py ligand bonded to the "Fe^{II}" ion. The mixed-valence Fe_3O acetate complexes are found to be "valence localized" on the vibrational time scale at all temperatures as indicated by variable-temperature IR data.

Trinuclear, oxo-centered, carboxylate complexes of transition metals have been of interest for several years. There is no ongoing discussion[3-5] about how to explain the variable-temperature magnetic susceptibility characteristics of salts of $[M_3O(O_2CR)_6(H_2O)_3]^+$, where M is either Fe^{III} or Cr^{III}. There have been suggestions that the theoretical model to explain the magnetic exchange interactions present in these complexes requires a temperature-dependent distortion of the complex.[3] The presence of *inter*molecular interactions has also been suggested.[5] Time-resolved optical spectroscopy experiments have not only eloquently demonstrated that there are two different triangular $Cr_3^{III}O$ complexes in $[Cr_3O(O_2CCH_3)_6(H_2O)_3]Cl\cdot 6H_2O$ at low temperatures but have also provided clear evidence for excitation energy transfer between the two different $Cr_3^{III}O$ complexes in the solid state.[6] Heat capacity experiments[7] have clearly demonstrated the presence of a phase transition in this $Cr_3^{III}O$ complex, corresponding to an order–disorder transition involving the H_2O solvate molecules.

Single-crystal X-ray structures have been reported for several mixed-valence, trinuclear acetate complexes. The complex $Ru_3O(O_2CCH_3)_6(PPh_3)_3$ has been indicated to have threefold symmetry at room temperature.[8] In a preliminary communication[9] of the room-temperature structure, $[Mn_3O(O_2CCH_3)_6(py)_3](py)$ (py = pyridine) has been shown to crystallize in $R32$. The presence of a C_3 axis indicated to the authors that all three manganese ions are equivalent. However, it should be pointed out that the pyridine solvate molecule was not located. A table in the review by Catterick and Thornton[10] indicates that $[Fe_3O(O_2CCH_3)_6(py)_3](py)$ is isostructural to the manganese complex. In another communication[11] $[Mn_3O(O_2CCH_3)_6(3\text{-Cl-py})_3]$ was described as valence trapped ($P2_1/a$ space group) with one Mn^{II} and two Mn^{III} ions. The atomic coordinates for this compound obtained from the Cambridge Crystallographic Data Centre show that there is a disordered 3-Cl-py solvate present as well. Recently, Cotton et al.[12-14] have reported the structures of analogous Cr_3O and V_3O complexes. $[Cr_3O(O_2CCF_2H)_6(py)_3]((C_2H_5)_2O)$ and $[Cr_3O(O_2CCF_2H)_6(4\text{-CN-py})_3](toluene)$ crystallize at room temperature in $R32$ and $R3c$, respectively. Again, the presence of threefold symmetry in each of these compounds as taken to

(1) University of Illinois.
(2) University of Texas.
(3) Jones, D. H.; Sams, J. R.; Thompson, R. C. *J. Chem. Phys.* **1984**, *81*, 440.
(4) Tsukerblat, B. S.; Belinskii, M. I.; Kuyavskaya, B. Ya. *Inorg. Chem.* **1983**, *22*, 995.
(5) (a) Wrobleski, J. T.; Dziobkowski, C. T.; Brown, D. B. *Inorg. Chem.* **1981**, *20*, 684. (b) Wrobleski, J. T.; Dziobkowski, C. T.; Brown, D. B. *ibid* **1981**, *20*, 671.
(6) (a) Schenk, K. J.; Gudel, H. U. *Inorg. Chem.* **1982**, *21*, 2253. (b) Dubicki, L.; Ferguson, J.; Williamson, B. *Inorg. Chem.* **1983**, *22*, 3220.
(7) Sorai, M.; Tachiki, M.; Suga, H.; Seki, S. *J. Phys. Soc. Jpn.* **1971**, *30*, 750.
(8) Cotton, F. A.; Norman, J. G. *Inorg. Chim. Acta* **1972**, *6*, 411.
(9) Baikie, A. R. E.; Hursthouse, M. B.; New, D. B.; Thornton, P. *J. Chem. Soc., Chem. Commun.* **1978**, 62.
(10) See Table III in: Catterick, J.; Thornton, P. *Adv. Inorg. Chem. Radiochem.* **1977**, *20*, 291.
(11) Baikie, A. R. E.; Hursthouse, M. B.; New, L.; Thornton, P.; White, R. G. *J. Chem. Soc., Chem. Commun.* **1980**, 684.
(12) Cotton, F. A.; Wang, W. *Inorg. Chem.* **1982**, *21*, 2675.
(13) Cotton, F. A.; Lewis, G. E.; Mott, G. N. *Inorg. Chem.* **1982**, *21*, 3127.
(14) Cotton, F. A.; Lewis, G. E.; Mott, G. N. *Inorg. Chem.* **1982**, *21*, 3316.

0002-7863/85/1507-8009$01.50/0

indicate that the three chromium ions are electronically equivalent as a result of electron delocalization. In one of two V_3O complexes, $[V_3(O)_3(O_2CC_6H_5)_6(THF)]$,[13] the V_3 triangle is quite asymmetric since the central oxygen atom is much closer to one vanadium atom than to the other two. In the other complex, the approximate D_{3h} symmetry in $[V_3O(O_2CCF_3)_6(THF)_3]$ suggests that the three vanadium atoms are electronically equivalent. When considering the X-ray diffraction studies it should be remembered that the time involved in collecting X-ray diffraction data is on the order of minutes per reflection and days per complete data set. It is not possible to tell whether a particular M_3O complex has a completely delocalized electronic structure with no barrier for intramolecular electron transfer or if the intramolecular electron transfer is faster than can be gauged in the time it takes to obtain diffraction data. For the complexes that appear to have a threefold symmetry the possibility of static and/or dynamic disorder also has to be considered.

Lupu et al.[15] first reported that the complexes $[Fe_3O(O_2CCH_3)_6L_3]$, where L is H_2O or pyridine, are mixed-valence complexes because they show Fe^{II} and Fe^{III} quadrupole-split doublets in their Mössbauer spectra at low temperatures. At room temperature, however, a single Mössbauer absorption is seen. The temperature dependences observed for the Mössbauer spectra of these two complexes and a few related complexes have been studied by a number of workers.[16-19] The most detailed Mössbauer study was reported by Brown et al.[20] Spectra at intermediate temperatures were simulated by a three-site relaxation model to give an activation energy of 470 cm^{-1}. This energy was taken by Brown et al. to be equal to the barrier to intramolecular thermal electron transfer. The question of valence delocalization in these mixed-valence Fe_3O acetates has also been examined with variable-temperature IR spectroscopy.[21] Finally, three theoretical treatments of the vibronic nature of the mixed-valence M_3O complexes have pointed to interesting possibilities of intermediate states.[22-24]

In a recent communication[25] we showed that the solvate molecule dramatically affects the electron-transfer rate in the *solid state* for $[Fe_3O(O_2CCH_3)_6(py)_3]$(solvate), where the solvate molecule can be a variety of molecules such as pyridine or benzene. The single-crystal X-ray structural results obtained at 163 and 298 K were also communicated for one of these trinuclear mixed-valence complexes. It was found that the Fe_3 triangle becomes more equilateral as the crystal is heated from 163 to 298 K. In this paper results will be given that indicate it is a dynamic disorder of certain ligands and/or solvate molecules that controls the rate of intramolecular electron transfer in the solid state. An overview[26] of progress in this area has very recently been published.

Experimental Section

Physical Measurements. Variable-temperature ^{57}Fe Mössbauer spectra were obtained in vertical transmission geometry by using a constant acceleration spectrometer that has been described before.[27] The source originally consisted of 50 mCi of ^{57}Co diffused into a 12-μm rhodium matrix. Temperature control is by means of a Lake Shore Cryotronics Model DTC-500-SP temperature controller. Sample temperature measurements are made with a calibrated Allen Bradley 560 Ω, W carbon resistor mounted in the copper sample cell holder. The estimated accuracy of absolute sample temperature determination is ±1 K below 10 K, better than ±2 K for the 10–30 K region and ±3 K for temperatures above ~30 K. The *relative* precision of temperature determination is ±0.5 K at the higher temperatures. Isomer shift data are reported relative to iron foil at 298 K but are not corrected for temperature-dependent second-order Doppler effects. It should be noted that isomer shifts illustrated in the figures are displaced slightly from the actual values, whereas accurate isomer shift values are to be found in the tabulated results. Computer fittings of the Mössbauer data to Lorentzian line shapes were carried out with a modified version of a previously reported computer program.[28] Nicolet Model 5 MX FT-IR and Perkin-Elmer Model 599B spectrophotometers were used to obtain infrared spectra of samples prepared as KBr pellets. Variable-temperature (50–300 K) IR data were obtained with use of a Spectrim Model 20170 closed-cycle refrigerator (Cryogenic Technology, Inc.).

Compound Preparations. Pyridine and 4-ethylpyridine (4-Et-py) were dried by refluxing with BaO and fractional distillation under vacuum. Acetonitrile was dried over P_2O_5 and distilled under an argon atmosphere. All elemental analyses were performed in the Microanalytical Laboratory of the School of Chemical Sciences, University of Illinois. Dried samples of compounds were always stored and manipulated in an inert-atmosphere glove box under an argon atmosphere.

$[Fe_3O(O_2CCH_3)_6(H_2O)_3]$. This mixed-valence compound was prepared by a previously reported method.[21] $FeCl_2 \cdot 4H_2O$ (20 g, 0.1 mol), 20 g (0.24 mol) of sodium acetate, and 60 g (1 mol) of glacial acetic acid were dissolved in 100 mL of water. The reaction mixture was heated at 70–80 °C under reflux for 2 h, while bubbling a constant stream of air. The mixture was cooled to room temperature and the drak-brown precipitate was filtered, washed with ethanol and ethyl ether, and then dried under vacuum. The yield was 10.4 g (52.7%).

$[Fe_3O(O_2CCH_3)_6(py)_3](py)$. Samples of this compound were prepared according to the method of Lupu and Ripan.[15b] $[Fe_3O(O_2CCH_3)_6(H_2O)_3]$ (5 g, 8.4 mmol) was dissolved in 30 mL of pyridine under argon atmosphere. The reaction mixture was stirred for 1 h at 50–60 °C and then slowly evaporated for 3 days. The black crystalline product was filtered off and dried under vacuum (yield 5.6 g (78%)). Anal. Calcd for $C_{32}Fe_3H_{38}N_4O_{13}$: C, 44.99; Fe, 19.61; H, 4.49; N, 6.56. Found: C, 45.00; Fe, 19.58; H, 4.34; N, 6.32.

$[Fe_3O(O_2CCH_3)_6(4\text{-Et-py})_3](4\text{-Et-py})$. This compound was prepared by the same method as was used for the above pyridine compound. Crystals suitable for X-ray crystallography were grown by slow evaporation of a 4-ethylpyridine solution under an argon atmosphere. Anal. Calcd for $C_{40}Fe_3H_{54}N_4O_{13}$: C, 49.71; Fe, 17.34; H, 5.63; N, 5.80. Found: C, 49.72; Fe, 17.56; H, 5.61; N, 5.71.

$[Fe_2CoO(O_2CCH_3)_6(py)_3](py)$. $Fe(NO_3)_3 \cdot 9H_2O$ (8.08 g, 0.02 mol), 2.91 g (0.01 mol) of $Co(NO_3)_2 \cdot 6H_2O$, and 16.5 g (0.2 mol) of NaO_2CCH_3 were dissolved in 60 mL of water and stirred for 1 day at room temperature. The brown precipitate was filtered and washed with ethanol and ethyl ether. The product was dried under vacuum for 3 days; the yield was 4.45 g (74.8%). $Fe_2CoO(O_2CCH_3)_6(H_2O)_3$ (4 g, 6.7 mmol) was dissolved in 50 mL of pyridine and slowly evaporated for 4 days. The black crystalline product was filtered and dried under vacuum; the yield was 4.21 g (73.3%). Anal. Calcd for $C_{32}Co_1Fe_2H_{38}N_4O_{13}$: C, 44.83; Co, 6.87; Fe, 13.03; H, 4.47; N, 6.54. Found: C, 44.94; Co, 6.95; Fe, 13.02; H, 4.51; N, 6.77.

$[Cr_2FeO(O_2CCH)_6(py)_3](py)$. $Fe_3O(O_2CCH_3)_6(H_2O)_3$ (0.88 g, 1.49 mmol) and 0.66 g (1.75 mmol) of $Cr_2(O_2CCH_3)_4 \cdot 2H_2O$, which was prepared according to the method of Kranz and Witkowska,[29] were dissolved in 50 mL of pyridine and stirred for 3 h at 50–60 °C and then slowly evaporated for 4 days. The black crysalline product was filtered and dried under vacuum; the yield was 0.44 g (29.17%). Anal. Calcd for $C_{32}Cr_2Fe_1H_{38}N_4O_{13}$: C, 45.40; Cr, 12.29; Fe, 6.60; H, 4.52; N, 6.62. Found: C, 45.46; Cr, 12.2; Fe, 6.96; H, 4.37; N, 6.51.

$[Fe_3O(O_2CCH_3)_6(4\text{-Et-py})_3]ClO_4$. $[Fe_3O(O_2CCH_3)_6(H_2O)_3]ClO_4$ (0.3 g, 0.43 mmol), which was prepared according to the literature,[5] was dissolved in 30 mL of ethanol and 0.05 g of $NaClO_4 \cdot H_2O$ and 20 mL of 4-ethylpyridine were added. The resulting yellowish green solid (0.34 g) was collected by filtration, washed with a small amount of ethanol, and then dried. Anal. Calcd for $C_{33}Fe_3H_{45}N_3O_{17}Cl$: C, 41.34; Fe, 17.84;

(15) (a) Lupu, D. *Rev. Roum. Chim.* **1970**, *15*, 417. (b) Lupu, D.; Ripan, R. *Rev. Roum. Chim.* **1971**, *16*, 43. (c) Lupu, D.; Barb, D.; Filoti, G.; Morariu, M.; Tarina, D. *J. Inorg. Nucl. Chem.* **1972**, *34*, 2803. (d) Grecu, R.; Lupu, D. *Rev. Roum. Chim.* **1971**, *16*, 1811.
(16) Turte, K. I.; Bobkova, S. A.; Stukan, R. A. *Z. Neorgan. Khim.* **1984**, *29*, 731.
(17) Stukan, R. A.; Turte, K. I.; Ablov, A. B.; Bobkova, S. A. *Koord. Khim.* **1979**, *5*, 95.
(18) Turte, K. I.; Bobkova, S. A.; Stukan, R. A.; Dorogan, A. V.; Veksel'man, M. E. *Koord. Khim.* **1982**, *8*, 794.
(19) Gol'danskii, V. I.; Alekseev, V. P.; Stukan, R. A.; Turte, K. I.; Ablov, A. V. *Dokl. Akad. Nauk SSSR* **1973**, *213*, 867.
(20) Dziobkowski, C. T.; Wrobleski, J. T.; Brown, D. B. *Inorg. Chem.* **1981**, *20*, 679.
(21) Johnson, M. K.; Cannon, R. D.; Powell, D. B. *Spectrochim. Acta* **1982**, *38A*, 307.
(22) Cannon, R. D.; Montri, L.; Brown, D. B.; Marshall, K. M.; Elliott, C. M. *J. Am. Chem. Soc.* **1984**, *106*, 2591.
(23) Borshch, S. A.; Kotov, I. N.; Bersuker, I. B. *Chem. Phys. Lett.* **1982**, *89*, 381.
(24) Launay, J. P.; Babonneau, F. *Chem. Phys.* **1982**, *67*, 295.
(25) Oh, S. M.; Hendrickson, D. N.; Hassett, K. L.; Davis, R. E. *J. Am. Chem. Soc.* **1984**, *106*, 7984.
(26) Hendrickson, D. N.; Oh, S. M.; Dong, T.-Y.; Kambara, T.; Cohn, M. J.; Moore, M. F. *Comments Inorg. Chem.*, in press.
(27) Cohn, M. J.; Timken, M. D.; Hendrickson, D. N. *J. Am. Chem. Soc.* **1984**, *106*, 6683.
(28) Münck, E.; Groves, J. L.; Tumolillo, T. A.; Debrunner, P. G. *Comput. Phys. Commun.* **1973**, *5*, 225.
(29) Kranz, M.; Witkowska, A. *Inorg. Synth.* **1960**, *6*, 144.

H, 4.73;, N, 4.38; Cl, 3.70. Found: C, 41.31; Fe, 17.54; H, 4.69; N, 4.32; Cl, 3.75.

$[Fe_2CoO(O_2CCH_3)_6(4\text{-Et-py})_3](4\text{-Et-py})$. This compound was prepared according to the same method used for the pyridine analogue. Anal. Calcd for $C_{40}Co_1Fe_2H_{54}N_4O_{13}$: C, 49.55; Co, 6.08; Fe, 11.52; H, 5.61; N, 5.78. Found: C, 48.98; Co, 6.1; Fe, 11.61; H, 5.63; N, 5.83.

$[Fe_3O(O_2CCH_3)_6(py)_3](benzene)$ and **$[Fe_3O(O_2CCH_3)_6(py)_3]$** were prepared by recrystallizing $[Fe_3O(O_2CCH_3)_6(py)_3](py)$ in benzene and CH_3CN, respectively. Anal. Calcd for $[Fe_3O(O_2CCH_3)_6(py)_3](benzene)$: C, 46.45; Fe, 19.64; H, 4.61; N, 4.92. Found: C, 46.35; Fe, 19.84; H, 4.63; N, 4.76. Calcd for $[Fe_3O(O_2CCH_3)_6(py)_3]$: C, 41.84; Fe, 21.62; H, 4.29; N, 5.42. Found: C, 41.21; Fe, 21.60; H, 4.19; N, 5.53.

Crystallographic Analysis. For each experiment a single crystal was affixed to a glass fiber attached to a goniometer head and then transferred to the automated diffractometer. For the determination at 298 K, the crystal was coated with a film of epoxy cement to eliminate the otherwise rapid loss of solvent and loss of crystallinity. In the low-temperature study, the crystal was maintained in a cold stream of dry nitrogen (163 K) for the duration of the diffraction experiments; at this temperature there was no evidence of crystal deterioration. Preliminary diffraction studies allowed determination of crystal symmetry and verification of the suitable quality of the crystals for intensity data collection. A summary of the pertinent crystal data and details of the X-ray diffraction data collection and processing are presented in Table I. The measured intensities were reduced and assigned standard deviations as described elsewhere,[30] including correction for absorption based on measured crystal shape for the 163 K study. Since the crystal used at 298 K was covered with epoxy cement, its shape could not be reliably measured, so no absorption correction was applied; the small range of transmission factors calculated for the 163 K study suggests that the neglected absorption correction at 298 K is small.

Solution and Refinement of the Structures. Each structure was solved by the heavy-atom method, using heavy-atom positions determined from a sharpened Patterson map. All structures were refined by full-matrix least-squares methods, using the program SHELX. Neutral atom scattering factors[31] for H, C, N, O, and Fe were used, including real and imaginary corrections for anomalous dispersion.

Since the two space groups *Cc* (No. 9) and *C2/c* (No. 15) are not distinguishable on the basis of systematic absences, a careful attempt was made to solve and refine the 163 K structure in the noncentrosymmetric *Cc*, where crystallographic symmetry would not impose any molecular symmetry (and no necessary ligand disorder). These least-squares calculations were characterized by extreme oscillations in many parameters, a failure to converge satisfactorily even after many cycles and extreme damping of shifts, differences of up to 0.2 Å between chemically equivalent bonds, and several nonpositive definite temperature factors. The unsuccessful refinement was therefore abandoned, and the centrosymmetric space group *C2/c* allowed smooth and satisfactory refinement at both temperatures. The molecule occupies the crystallographic twofold axis at $0,y,^1/_4$, with one iron atom (Fe1) and the oxo bridge on this axis. Significantly (see discussion of disorder transition below), the 4-Et-py ligand (N1 and C7–C13) attached to this iron atom is disordered, with N1 and C9 not lying on the axis, as originally expected. The structure also contains one non-light molecule of 4-Et-py per complex molecule. This solvate molecule (N101, C102–108) is disordered about a center of inversion.

For the refinement at 163 K, it was possible to refine all non-H atoms anisotropically. Hydrogen atoms on the disordered solvate molecule were placed in calculated ideal positions, with fixed *U* values. All other hydrogen atoms could be positionally refined except those on the ethyl group of the disordered ligand, so these latter were omitted from the calculation. For hydrogen atoms on the well-behaved ligand (N1, C14–C20), thermal parameters could be refined, but that of each of the remaining hydrogen atoms (on the ring of the disordered 4-Et-py and on the bridging acetato ligands) was fixed equal to the equivalent isotropic thermal parameter of the carbon atom to which it was attached.

In the 298 K refinement carbon and nitrogen atoms of the disordered solvate molecule were refined isotropically. Refinement of hydrogen atoms was similar to that in the 163 K structure, except that the *U* values assigned to hydrogen atoms on the disordered 4-Et-py and on the bridging acetate ligands represented average values for that environment.

For each structure, refinement was continued until shifts in all parameters were less than one estimated standard deviation in the respective parameter. Further details of the refinements appear in Table I. Observed and calculated structure amplitudes, final crystallographic coordinates and thermal parameters, and full tables of bond lengths, bond angles are given in the supplementary material.[32]

Table I. Crystallographic Summary at 163 and 298 K

	163 K	298 K
	A. Crystal Data[a]	
a, Å	17.060 (6)	17.142 (3)
b, Å	16.943 (7)	17.004 (1)
c, Å	16.183 (8)	16.571 (4)
α, deg	90.0	90.0
β, deg	104.49 (4)	104.27 (2)
γ, deg	90.0	90.0
V, Å^3	4526.6	4681.1
d_{calcd}, g cm^{-3} (−110 °C)	1.418	1.371
empirical formula	$Fe_3C_{40}H_{54}O_{13}N_4$	$Fe_3C_{40}H_{54}O_{13}N_4$
fw	966.42	966.42
crystal system	monoclinic	monoclinic
space group	*C2/c*	*C2/c*
Z	4	4
F(000), electrons	2016	2016
	B. Data Collection[b]	
radiation, λ (Å)	Mo Kα, 0.71069	Mo Kα, 0.71069
mode	ω scan	ω scan
scan range	symmetrically over 1.0° about $K\alpha_{1,2}$ max	
background	offset 1.0 and −1.0° in ω from $K\alpha^{1,2}$ max	
2θ range, deg	4.0–55.0	4.0–55.0
scan rate, deg min^{-1}	2.0–6.0	3.0
exposure time, h	97.2	59.0
total reflections measd	5202	5387
absorption coeff (Mo Kα), cm^{-1}	10.4	10.4
transmission factor range	0.820–0.857	
	C. Structure Refinement[c]	
ignorance factor, *p*	0.04	0.04
reflections used, $F > 6(\sigma_F)$	2847	2809
no. of variables	359	293
goodness of fit	1.48	2.22
R, wR[b]	0.0457, 0.0425	0.0525, 0.0546
R for all data	0.100	0.110
max shift/esd	0.28	0.22

[a] Unit cell parameters were obtained by least-squares refinement of the setting angles at 163 K of 45 reflections with $20.2 < 2\theta < 24.3°$ and at 298 K of eight equivalent settings each for 19 reflections with $20.1 < 2\theta < 28.3°$. [b] Syntex $P2_1$ autodiffractometer with a graphite monochromator and a Syntex LT-1 inert-gas (N_2) low-temperature delivery system for the 163 K data; Picker diffractometer automated by Krisel Controls for the 298 K data. Data reduction was carried out as described: Riley, P. E.; Davis, R. E. *Acta Crystallogr., Sect. B* **1976**, *32*, 381. Crystal and instrument stability were monitored by remeasurement of 4 check reflections after every 96 reflections. These data were analyzed as detailed by Henslee and Davis: Henslee, W. H.; Davis, R. E. *Acta Crystallogr., Sect. B* **1975**, *31*, 1511. [c] Relevant expressions are as follows, where in this footnote F_o and F_c represent respectively the observed and calculated structure factor amplitudes. Function minimized was $\Sigma w(F_o - F_c)^2$, where $w = (\sigma_F)^{-2}$, $R = \Sigma abs(F_o - F_c)/\Sigma F_o$, $wR = (\Sigma w(F_o - F_c)^2/\Sigma wF_o^{2\,1/2}$. The computer programs used in the data reduction and in the structure refinement and analysis are as previously detailed: Gadol, S. M.; Davis, R. E. *Organometallics* **1982**, *1*, 1607.

Results and Discussion

Effect of Solvate Molecule. Several new series of mixed-valence complexes of the composition $[Fe_3O(O_2CCH_3)_6L_3](solvate)$ have been prepared, where L is pyridine (py) or a substituted pyridine. In each series the ligand L is kept constant while the solvate molecule is varied. The Mössbauer results for $[Fe_3O(O_2CCH_3)_6(py)_3](py)$, $[Fe_3O(O_2CCH_3)_6(py)_3]$, and $[Fe_3O(O_2CCH_3)_6(py)_3](benzene)$ are presented in this paper. Data for other series will be presented in forthcoming papers.

(30) Riley, R. E.; Davis, R. E. *Acta Crystallogr., Sect. B* **1976**, *32*, 381.
(31) Scattering factors for H, C, N, and O atoms were used as programmed in SHELX-76. Values for the Fe atoms were obtained from "International Tables for X-Ray Crystallography"; Kynoch Press: Birmingham, England, 1974; Vol. IV.
(32) See the note at the end of the paper regarding the availability of supplementary material.

Table II. Iron-57 Mössbauer Fitting Parameters for $[Fe_3O(O_2CCH_3)_6(py)_3]$[a]

T, K	δ,[b] mm/s		ΔE_Q, mm/s		Γ,[c] mm/s		area ratio
	Fe^{III}	Fe^{II}	Fe^{III}	Fe^{II}	Fe^{III}	Fe^{II}	Fe^{III}/Fe^{II}
120 (1)	0.515 (1)	1.246 (1)	1.010 (1)	1.223 (2)	0.125 (1)	0.126 (1)	1.99 (2)
					0.131 (1)	0.130 (2)	
179 (1)	0.503 (1)	1.222 (1)	1.014 (1)	1.124 (3)	0.129 (1)	0.129 (2)	2.11 (5)
					0.136 (1)	0.132 (2)	
248 (1)	0.484 (1)	1.142 (2)	0.985 (2)	0.957 (3)	0.132 (2)	0.123 (3)	2.27 (6)
					0.145 (2)	0.132 (3)	
315 (1)	0.434 (1)	1.102 (2)	0.962 (2)	0.893 (4)	0.132 (2)	0.123 (3)	2.25 (8)
					0.153 (2)	0.143 (3)	

[a] Peaks were least-squares fit to Lorentzian line shapes with equal areas for both components of a doublet. The error in the last significant figure is given in parentheses. [b] Center shifts relative to Fe metal. [c] Half-width at half-maximum listed in order of increasing velocity of the peak.

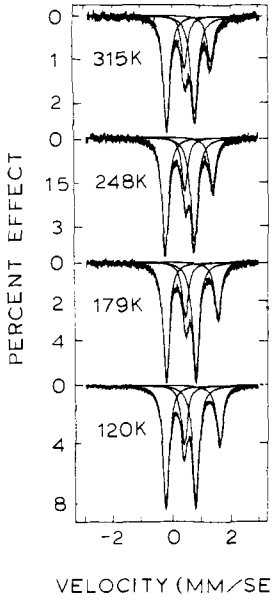

Figure 1. Variable-temperature ^{57}Fe Mössbauer spectra for $[Fe_3O(O_2CCH_3)_6(py)_3]$.

Examination of Figures 1–3 shows that changing the solvate molecule in $[Fe_3O(O_2CCH_3)_6(py)_3]$(solvate) has a dramatic effect on the intramolecular electron-transfer rate in the mixed-valence Fe_3O complex. In Figure 1 are illustrated Mössbauer spectra for $[Fe_3O(O_2CCH_3)_6(py)_3]$ at several temperatures from 120 to 315 K. Least-squares fitting of these spectra with Lorentzian line shapes clearly indicates that only two quadrupole-split doublets are present in each spectrum. The less intense doublet is that for the Fe^{II} ion, whereas the other doublet arises from the two Fe^{III} ions. The area ratio of Fe^{III} to Fe^{II} doublets is 2.0 at 120 K and increases slightly to 2.25 at 315 K. Table II summarizes the center shifts (δ) and quadrupole splittings (ΔE_Q) obtained by fitting the spectra in Figure 1. It is clear that $[Fe_3O(O_2CCH_3)_6(py)_3]$ remains valence localized on the Mössbauer time scale up to a temperature of 315 K. The intramolecular electron-transfer rate is less than $\sim 10^7$ s^{-1}. The small variations in δ and ΔE_Q as a function of temperature are what is expected for high-spin Fe^{II} and Fe^{III} ions that are not involved in an electron transfer. Verification for this can be seen in Figure 4 where variable-temperature Mössbauer data for $[Fe_2^{III}Co^{II}O(O_2CCH_3)_6(py)_3](py)$ and $[Cr_2^{III}Fe^{II}O(O_2CCH_3)_6(py)_3](py)$ are illustrated. The spectra for the former compound show one high-spin Fe^{III} doublet which is relatively temperature independent. Fitting parameters for these two compounds are given in Table III. The small temperature dependence seen for the single doublet in the $Cr_2^{III}Fe^{II}$ spectra is what is expected for a high-spin Fe^{II} ion. The $Cr_2^{III}Fe^{II}$ and $Fe_2^{III}Co^{II}$ complexes have the same type of solid-state structure as $[Fe_3O(O_2CCH_3)_6(py)_3](py)$, for the room-temperature powder X-ray diffraction (XRD) patterns of the three compounds are essentially superimposable.

In contrast to $[Fe_3O(O_2CCH_3)_6(py)_3]$, the Mössbauer spectrum of $[Fe_3O(O_2CCH_3)_6(py)_3](py)$ shows a pronounced temperature dependence (see Figure 2). At temperatures below ~ 100 K two doublets are seen, one for the high-spin Fe^{II} ion and a second doublet with twice the area and parameters characteristic of

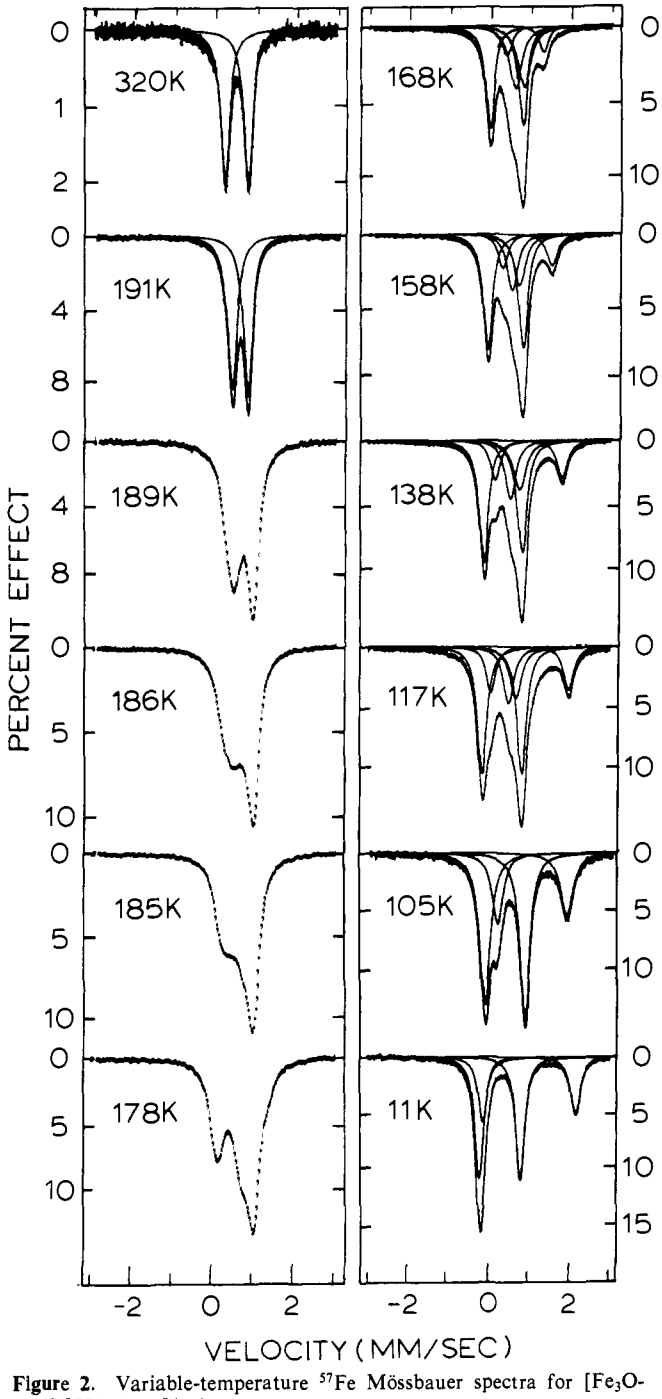

Figure 2. Variable-temperature ^{57}Fe Mössbauer spectra for $[Fe_3O(O_2CCH_3)_6(py)_3](py)$.

Table III. Iron-57 Mössbauer Fitting Parameters[a] for Two Mixed-Metal Oxo-Centered Acetates

	δ,[b] mm/s		ΔE_Q, mm/s		Γ,[c] mm/s	
T, K	Fe^{III}	Fe^{II}	Fe^{III}	Fe^{II}	Fe^{III}	Fe^{II}
			$[Fe_2^{III}Co^{II}O(O_2CCH_3)_6(py)_3](py)$			
120 (1)	0.517 (1)		1.105 (1)		0.127 (1)	0.130 (2)
160 (1)	0.510 (1)		1.101 (1)		0.124 (1)	0.126 (2)
199 (1)	0.504 (1)		1.092 (1)		0.121 (2)	0.124 (2)
237 (1)	0.501 (1)		1.090 (2)		0.121 (2)	0.118 (2)
296 (1)	0.493 (1)		1.081 (2)		0.122 (2)	0.123 (2)
			$[Cr_2^{III}Fe^{II}O(O_2CH_3)_6(py)_3](py)$			
100 (1)		1.250 (1)		1.582 (2)		0.130 (1) 0.127 (2)
149 (1)		1.227 (1)		1.440 (2)		0.127 (1) 0.127 (2)
190 (1)		1.194 (1)		1.373 (2)		0.124 (2) 0.126 (2)
247 (1)		1.146 (1)		1.324 (2)		0.126 (2) 0.123 (2)
297 (1)		1.114 (1)		1.203 (3)		0.122 (2) 0.122 (2)

[a] Peaks were least-squares fit to Lorentzian line shapes with equal areas for both components of a doublet; error in the last significant figure in parentheses. [b] Center shifts relative to Fe metal. [c] Half-width at half-maximum listed in order of increasing velocity of the peak.

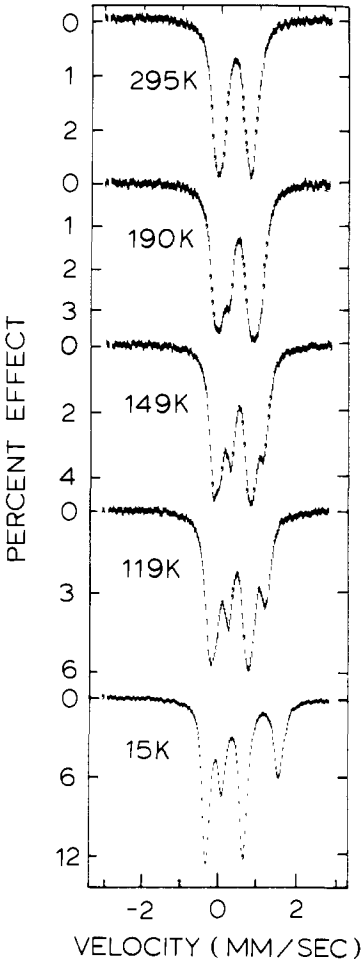

Figure 3. Variable-temperature ^{57}Fe Mössbauer spectra for $[Fe_3O(O_2CCH_3)_6(py)_3](benzene)$.

high-spin Fe^{III}. Parameters resultant from least-squares fitting several of the spectra to Lorentzian line shapes are given in Table IV. The solid lines in Figure 2 illustrate these fits. In the intermediate range it is not possible to get good fits of a spectrum to Lorentzian line shapes. As the temperature of this pyridine solvate is increased the spectrum changes to become a single average doublet at temperatures above ~200 K. In the high-temperature region the intramolecular electron transfer is occurring rapidly compared to the Mössbauer time scale. It should be pointed out that Stukan et al.[17] reported Mössbauer spectra for $[Fe_3O(O_2CCH_3)_6(py)_3](py)$ in the range of 80–300 K. They observed the same type of temperature dependence; however, their spectra were of poorer quality and their sample had ~12% of the

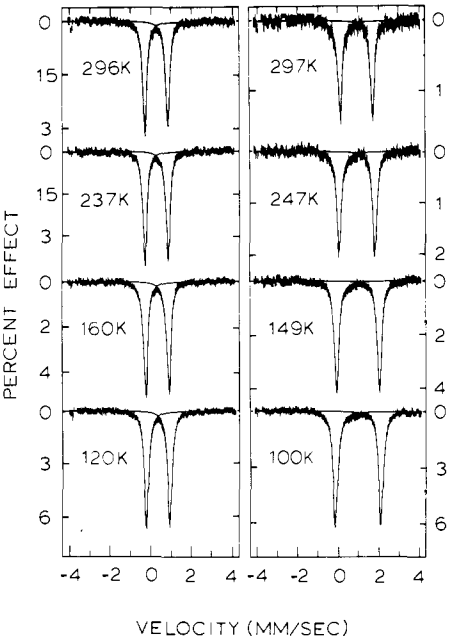

Figure 4. Variable-temperature ^{57}Fe Mössbauer spectra for the following: left panel, $[Fe_2^{III}Co^{II}O(O_2CCH_3)_6(py)_3](py)$; right panel, $[Cr_2^{III}Fe^{II}O(O_2CCH_3)_6(py)_3](py)$.

$Fe_3^{III}O$ acetate impurity. No detailed explanation of what is occurring was offered. Brown et al.[20] reported four very poorly resolved spectra (50–200 K) for a compound they characterized as the hemi-solvate $[Fe_3O(O_2CCH_3)_6(py)_3]^{1/2}(py)$. It is likely that this sample was a mixture of the solvated and non-solvated complexes.

Just how sensitive the *intra*molecular electron-transfer rate is for the molecule $Fe_3O(O_2CCH_3)_6(py)_3$ is evident in Figure 3 which shows Mössbauer spectra for $[Fe_3O(O_2CCH_3)_6(py)_3](benzene)$. Naively, the same Mössbauer characteristics would have been expected for this benzene solvate as are seen for the pyridine solvate because the two solvate molecules are of similar dimensions. A comparison of the spectra in Figures 2 and 3 shows that the benzene solvate does convert from valence localized to valence delocalized as the temperature is increased. However, the temperature dependencies of the spectra for the two compounds are different. It was found not to be possible to fit the Mössbauer spectra of the benzene solvate taken in the range of 119–295 K to Lorentzian line shapes. This could be due to the fact that several lines are overlapping, compounded perhaps by the presence of more than one Fe^{III} site as evidenced by the excess line width in the Fe^{III} signals. We have found that the room-temperature XRD patterns of the pyridine and benzene solvates are quite different.

Single-Crystal X-ray Structure of $[Fe_3O(O_2CCH_3)_6(4\text{-Et-py})_3](4\text{-Et-py})$. The molecular and solid-state structures of this

Table IV. Mössbauer Fitting Parameters for $[Fe_3O(O_2CCH_3)_6(py)_3](py)$[a]

	δ,[b] mm/s			ΔE_Q, mm/s			% area			Γ,[c] mm/s		
T, K	Fe^{III}	Fe^{av}	Fe^{II}	Fe^{III}	Fe^{av}	Fe^{II}	Fe^{III}	Fe^{av}	Fe^{II}	Fe^{III}	Fe^{av}	Fe^{II}
11 (1)	0.521 (1)		1.260 (2)	1.012 (2)		2.101 (2)	65.2 (1)		34.8 (1)	0.124 (1)		0.124 (1)
										0.131 (1)		0.129 (1)
51 (3)	0.529 (1)		1.221 (2)	1.013 (2)		1.902 (3)	64.4 (2)		35.6 (2)	0.147 (1)		0.151 (1)
										0.142 (1)		0.142 (2)
105 (1)	0.542 (1)		1.221 (2)	0.989 (1)		1.726 (3)	67.2 (1)		32.8 (1)	0.158 (1)		0.165 (2)
										0.145 (2)		0.186 (3)
106 (0.5)	0.541 (1)		1.220 (2)	0.994 (2)		1.731 (3)	65.4 (1)		34.6 (1)	0.155 (1)		0.176 (3)
										0.143 (1)		0.199 (4)
109 (0.5)	0.544 (1)		1.218 (2)	0.994 (2)		1.690 (3)	66.8 (1)		33.2 (2)	0.164 (1)		0.187 (4)
										0.149 (1)		0.213 (5)
111 (0.5)	0.544 (1)		1.225 (2)	0.993 (2)		1.672 (3)	67.2 (1)		32.6 (2)	0.164 (1)		0.191 (4)
										0.145 (1)		0.220 (5)
112 (0.5)	0.542 (1)	0.901 (2)	1.224 (2)	0.968 (2)	0.274 (5)	1.876 (3)	50.2 (2)	30.4 (2)	19.4 (2)	0.152 (2)	0.162 (2)	0.160 (4)
										0.144 (1)	0.174 (2)	0.186 (5)
113 (0.5)	0.545 (1)	0.893 (2)	1.224 (2)	0.962 (2)	0.221 (4)	1.821 (3)	48.6 (2)	33.0 (2)	18.4 (2)	0.148 (2)	0.164 (2)	0.150 (3)
										0.144 (1)	0.178 (2)	0.170 (4)
115 (0.5)	0.545 (1)	0.882 (2)	1.224 (2)	0.961 (2)	0.209 (4)	1.778 (3)	48.0 (2)	34.0 (2)	18.0 (2)	0.148 (2)	0.160 (2)	0.152 (3)
										0.143 (1)	0.176 (2)	0.168 (4)
117 (0.5)	0.547 (1)	0.870 (3)	1.213 (2)	0.960 (2)	0.231 (5)	1.701 (3)	47.0 (2)	32.0 (2)	21.0 (2)	0.142 (1)	0.156 (2)	1.154 (2)
										0.142 (1)	0.172 (3)	0.158 (2)
138 (1)	0.552 (1)	0.861 (3)	1.201 (2)	0.941 (3)	0.230 (6)	1.651 (3)	52.0 (2)	29.0 (2)	19.0 (2)	0.134 (1)	0.158 (2)	0.147 (2)
										0.147 (2)	0.187 (3)	0.156 (2)
158 (1)	0.589 (1)	0.845 (2)	1.130 (2)	0.867 (2)	0.214 (4)	1.216 (3)	52.8 (2)	30.0 (2)	17.2 (2)	0.135 (1)	0.156 (2)	0.147 (2)
										0.136 (1)	0.171 (2)	0.158 (3)
168 (1)	0.599 (1)	0.813 (3)	1.046 (10)	0.805 (3)	0.217 (5)	0.976 (14)	56.0 (2)	41.2 (2)	12.8 (2)	0.132 (1)	0.184 (2)	0.147 (2)
										0.132 (1)	0.188 (3)	0.132 (2)
191 (1)		0.743 (1)			0.520 (1)			100			0.189 (4)	
											0.181 (4)	
297 (1)		0.772 (1)			0.761 (2)			100			0.175 (4)	
											0.174 (4)	
320 (1)		0.753 (1)			0.760 (2)			100			0.169 (3)	
											0.164 (3)	

[a] Peaks were least-squares fit to Lorentzian line shapes with equal areas for both components of a doublet; error in the last significant figure is given in parentheses. [b] Center shifts relative to Fe metal. [c] Half-width at half-maximum listed in order of increasing velocity of the peak.

Table V. Distances[a] and Angles of the Central Atoms

	163 K		298 K	
atoms	A	deg	A	deg
Fe1-Fe2-Fe2*1	3.321 (2)	60.54 (2)	3.307 (1)	60.29 (2)
Fe2-Fe1-Fe2*1		58.92 (4)		59.42 (3)
Fe2-Fe2*1	3.267 (1)		3.276 (1)	
Fe1-O-Fe2	2.010 (4)	118.4 (1)	1.953 (5)	119.28 (2)
Fe2-O-Fe2*1	1.856 (7)	123.3 (2)	1.879 (2)	121.4 (2)
N1-Fe1-O	2.224 (5)	176.9 (7)	2.222 (6)	176.4 (1)
N1-Fe1-N1*1		6.2 (10)		7 (2)
Fe1-O1	2.093 (3)		2.069 (4)	
Fe1-O3	2.127 (3)		2.091 (4)	
N2-Fe2-O	2.230 (4)	177.3 (1)	2.227 (5)	178.7 (2)
Fe2-O2	2.037 (3)		2.050 (4)	
Fe2-O4	2.029 (3)		2.036 (4)	
Fe2-O5	2.078 (3)		2.072 (4)	
Fe2-O6	2.046 (3)		2.043 (4)	

[a] The distances refer to the first two atoms in each set of three. The suffix *1 on an atom label denotes transformation by $1 - x, y, 0.5 - z$.

complex were determined at 163 and 298 K by single-crystal X-ray diffraction techniques. Perspective drawings of the molecular structure of the oxo-centered $Fe_3O(O_2CCH_3)_6(4\text{-Et-py})_3$ complex deduced from the 163 and 298 K data sets are shown in Figure 5. Selected bond distances and angles for the central atoms of the Fe_3O triangle are given in Table V. The space group is $C2/c$ at both 163 and 298 K. At both temperatures there are two elements of disorder. The 4-Et-py solvate molecule is disordered about a center of inversion. As is visible in the plotting given in Figure 5, one 4-Et-py ligand is disordered on each complex. This disordered 4-Et-py ligand is coordinated to the unique iron ion located on the C_2 axis in the Fe_3O plane. In refining the structure it is necessary to split this 4-Et-py ligand between the two equivalent positions. Both of these two positions of the disordered 4-Et-py ligand are plotted in Figure 5. It is to be noted that the two 4-Et-py ligands which are not disordered have their planes perpendicular to the Fe_3O plane.

As the crystal is heated from 163 to 298 K significant dimensional changes occur in the Fe_3 triangle. Bond distances and angles of the Fe_3 triangle are given in Table V. The Fe_3 triangle becomes more equilateral as the crystal is heated from 163 to 298 K. At low temperatures the iron ion (Fe^A) which is located on the C_2 axis must be the high-spin Fe^{II} ion. At 163 K the bond distances to the central oxide ion are appreciably different: Fe^A–O = 2.010 (4) Å and Fe^B–O = 1.856 (7) Å. These two bond distances are closer to being equal in the 298 K structure: Fe^A–O = 1.953 (5) Å and Fe^B–O = 1.879 (2) Å. It is interesting that in going from 163 to 298 K the change in this bond length at the unique iron ion is negative and approximately twice as large (Fe^A–O = −0.057 Å) as the positive change seen at the other two iron ions (Fe^B–O = +0.023 Å). The symmetrizing of the Fe_3 triangle is also evident in Fe–Fe distances; the difference in the two different Fe–Fe distances is 0.054 Å at 163 K, and this difference shrinks to 0.029 Å at 298 K. The two different Fe–N bond lengths are essentially equal at both 163 and 298 K. Since the dimensions of the complex are changing so much from 163 to 298 K, it is very likely that the potential energy vs. nuclear coordinate plot for the ground state of this complex is also changing with temperature. It will be evident in the Mössbauer spectra for this complex (*vide infra*) that whatever the process is that leads to the changes in the Mössbauer spectra, this process is neither frozen out completely at 163 K nor completely averaged at 298 K.

A stereoview of the packing arrangement in the solid state at 163 K is shown in Figure 6. The $[Fe_3O(O_2CCH_3)_6(4\text{-Et-py})_3]$ complexes are well separated. There seems to be little opportunity for *inter*molecular electron transfer. It may be of importance that the disordered 4-Et-py solvate molecules are packed relatively close to the disordered 4-Et-py ligands. Due to the long time scale inherent in the collection of X-ray diffraction data, the structure obtained is one that is averaged over time (and, of course, over space as well). Thus, it is not possible to determine definitively from the X-ray results whether the disorder of 4-Et-py ligand (or

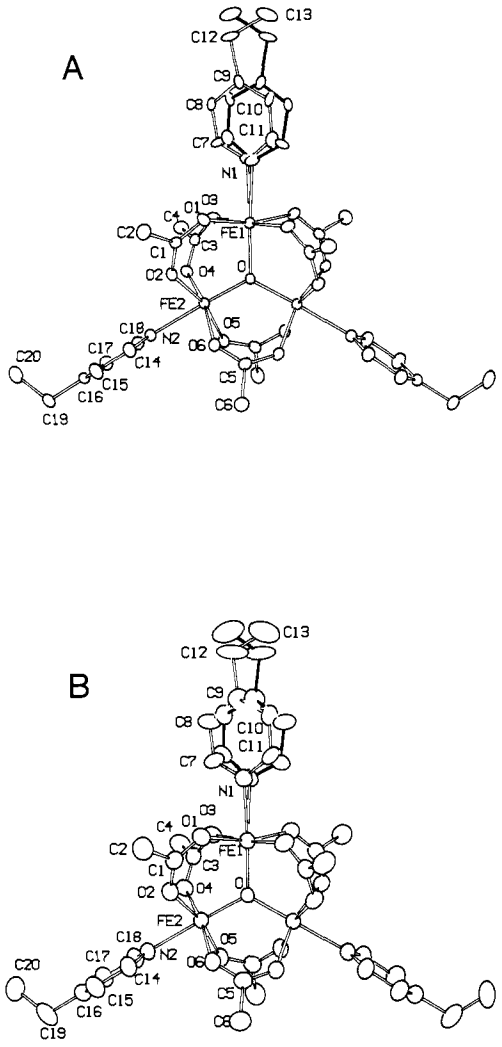

Figure 5. Perspective drawing of the molecular structure of $[Fe_3O(O_2CCH_3)_6(4\text{-Et-py})_3]$ in the compound $[Fe_3O(O_2CCH_3)_6(4\text{-Et-py})_3]$-(4-Et-py) at 163 (A) and 298 K (B). The two positions of the disordered 4-Et-py ligand are shown. Atoms are shown as 35% equiprobability ellipsoids.

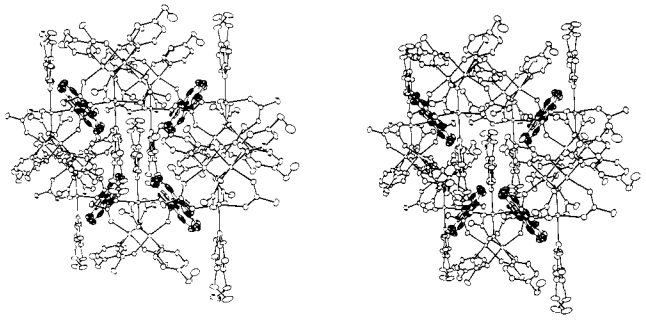

Figure 6. Stereoview showing the packing arrangement in $[Fe_3O(O_2CCH_3)_6(4\text{-Et-py})](4\text{-Et-py})$. The 4-Et-py solvate molecules are represented with shaded ellipsoids.

solvate) is static or dynamic. Large thermal parameters were found for the atoms of the disordered 4-Et-py ligand at 298 K, as can be seen in Figure 5. These relatively large thermal parameters are suggestive of dynamic disorder of this ligand. Perhaps at 298 K it is rapidly moving between the two limiting positions which are plotted in Figure 5, whereas at low temperatures (i.e., below 100 K) it is held fixed and is statically disordered throughout the lattice. Additional evidence to support the suggestion that the one disordered 4-Et-py ligand is changing from a static to a dynamic condition as the sample temperature is increased is

Table VI. Intermolecular Contact Distances Involving the 4-Et-py Ligands

atom 1	atom 2	sym[a]	d(163 K)	d(298 K)
(a) Involving the Disordered Ligand (up to 3.95 Å)				
N1	C15	a	3.91	4.16
C7	C20	a	3.93	4.24
C7	C15	b	3.94	3.88
C7	N101	c	3.76	3.80
C8	C20	c	3.73	3.80
C9	C15	b	3.93	4.12
C10	C15	b	3.88	4.09
C10	C106	b	3.93	4.12
C10	C15	b	3.88	4.09
C11	C15	a	3.94	4.07
C11	C15	b	3.86	3.94
C12	C106	b	3.73	3.74
C13	C106	a	3.86	4.13
(b) Involving the Ordered Ligand (up to 3.70 Å)				
C15	O1	d	3.62	3.73
C17	C3	e	3.58	3.68
C17	C4	e	3.46	3.52
C17	O4	e	3.58	3.63
C17	C5	f	3.36	3.38
C17	C6	f	3.61	3.66
C17	C7	f	3.61	3.66
C17	O6	f	3.61	3.62
C18	C4	e	3.54	3.68
C18	O4	e	3.46	3.58
C18	C5	f	3.46	3.54
C18	C6	f	3.46	3.58
C18	O5	f	3.44	3.45
C19	O3	g	3.70	3.80
C19	O1	d	3.70	3.85

[a] Atom 2 is transformed as follows, indicated by the notation in the sym column: a, $^1/_2 + x, -^1/_2 + y, z$; b, $^1/_2 - x, ^1/_2 + y, ^1/_2 - z$; c, $^1/_2 - x, ^1/_2 - y, -z$; d, $^1/_2 - x, ^1/_2 + y, ^1/_2 - z$; e, $1 - x, 1 - y, 1 - z$; f, $x, 1 - y, ^1/_2 + z$; g, $-^1/_2 + x, ^1/_2 + y, z$.

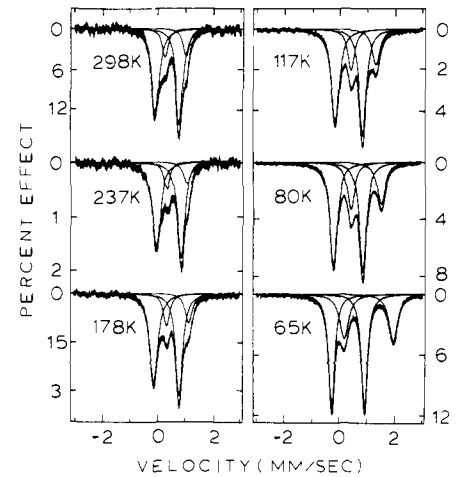

Figure 7. Variable-temperature ^{57}Fe Mössbauer spectra for $[Fe_3O(O_2CCH_3)_6(4\text{-Et-py})_3](4\text{-Et-py})$.

available from calculations of intermolecular contacts. Table VI gives the closest intermolecular contacts of the two crystallographically distinct ligands (not involving hydrogen atoms). At 163 K, no contacts of the disordered ligands are closer than 3.73 Å; a number of these become substantially longer at the higher temperature. By contrast, the ordered ligand is much more tightly held, with contacts as short as 3.36 Å at 163 K and 15 contact distances shorter than the shortest observed for the disordered ligand. Further, these show less pronounced lenghtening at the higher temperature. Inspection of the packing environment of the unique 4-Et-py ligand (Figure 6) suggests that it could move within this rather soft cavity, perhaps with some concomitant reorganization, in transit, of the solvate molecules. However, it is not possible to conclude from X-ray structural results alone that this is indeed occurring.

Table VII. Iron-57 Mössbauer Fitting Parameters for $[Fe_3O(O_2CCH_3)_6(4\text{-Et-py})_3](4\text{-Et-py})$[a]

T, K	δ,[b] mm/s		ΔE_Q, mm/s		Γ,[c] mm/s		area ratio
	Fe^{III}	Fe^{II}	Fe^{III}	Fe^{II}	Fe^{III}	Fe^{II}	Fe^{III}/Fe^{II}
6.5 (10)	0.551 (1)	1.304 (1)	1.192 (1)	1.783 (1)	0.133 (1)	0.193 (3)	1.94 (2)
					0.130 (1)	0.180 (3)	
30 (2)	0.555 (1)	1.308 (1)	1.193 (1)	1.714 (1)	0.135 (1)	0.195 (3)	1.95 (2)
					0.131 (1)	0.181 (3)	
50 (3)	0.554 (1)	1.304 (1)	1.181 (1)	1.640 (2)	0.135 (1)	0.194 (3)	1.99 (4)
					0.134 (1)	0.183 (4)	
80 (3)	0.557 (1)	1.280 (1)	1.160 (1)	1.461 (2)	0.148 (2)	0.195 (4)	2.01 (4)
					0.137 (2)	0.212 (4)	
117 (1)	0.566 (1)	1.192 (1)	1.072 (1)	1.112 (2)	0.155 (2)	0.178 (4)	2.08 (6)
					0.133 (2)	0.213 (5)	
178 (1)	0.576 (1)	1.075 (2)	0.994 (2)	0.882 (2)	0.170 (3)	0.168 (4)	2.25 (7)
					0.136 (2)	0.193 (5)	
237 (1)	0.579 (1)	0.954 (2)	0.940 (2)	0.801 (2)	0.175 (3)	0.171 (4)	2.50 (7)
					0.136 (2)	0.192 (4)	
298 (1)	0.587 (2)	0.853 (2)	0.891 (3)	0.773 (3)	0.179 (3)	0.142 (5)	3.55 (8)
					0.145 (2)	0.163 (5)	

[a] Peaks were least-squares fit to Lorentzian line shapes with equal areas for both components of a doublet; error in the last significant figure in parentheses. [b] Center shifts relative to Fe metal. [c] Half-width at half-maximum listed in order of increasing velocity of the peak.

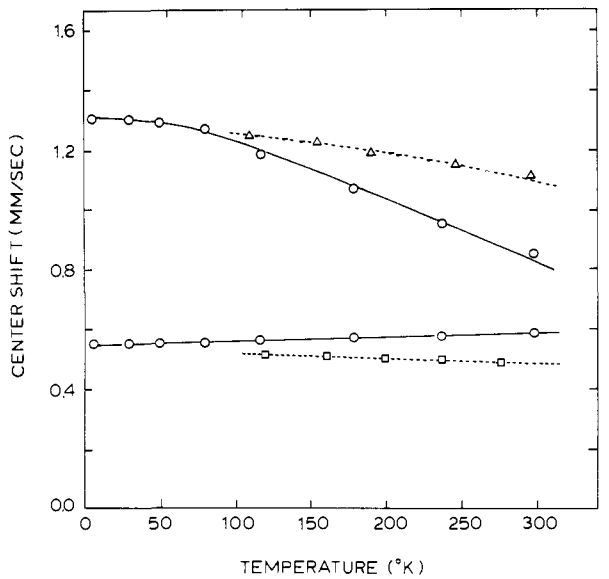

Figure 8. Plot of the center shift (δ) vs. temperature for the "Fe^{II}" and "Fe^{III}" doublets in the spectrum of $[Fe_3O(O_2CCH_3)_6(4\text{-Et-py})_3](4\text{-Et-py})$; data plotted as "O". Temperature dependence of center shifts: (Δ) $[Cr_2^{III}Fe^{II}O(O_2CCH_3)_6(py)_3](py)$; (□) $[Fe_2^{III}Co^{II}O(O_2CCH_3)_6(py)_3](py)$.

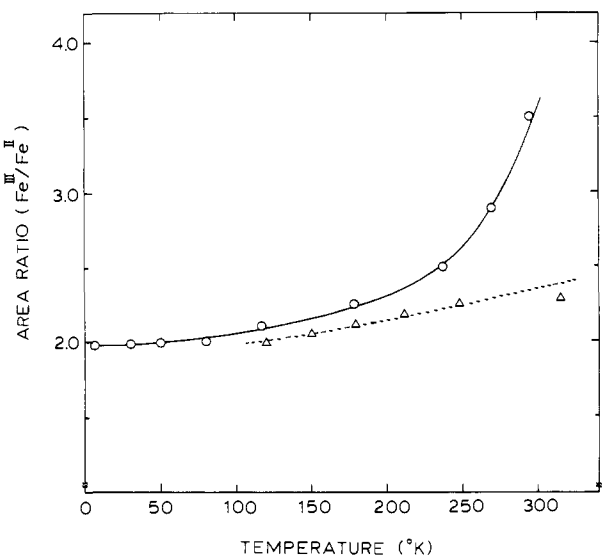

Figure 9. Plot of the area ratio of the "Fe^{III}" to "Fe^{II}" doublets as a function of temperature: (O) $[Fe_3O(O_2CCH_3)_6(4\text{-Et-py})_3](4\text{-Et-py})$; (Δ) $[Fe_3O(O_2CCH_3)_6(py)_3]$.

Physical Properties of $[Fe_3O(O_2CCH_3)_6(4\text{-Et-py})_3](4\text{-Et-py})$. In figure 7 are given some of the Mössbauer spectra run for this complex. At all temperatures least-squares fitting of the spectra indicates there are only two quadrupole-split doublets. At low temperatures the area ratio of the two doublets is 2:1. As can be seen from the fitting parameters given in Table VII, the less intense doublet is that for a high-spin Fe^{II} ion. The two high-spin Fe^{III} ions give rise to the more intense doublet. Three observations can be made from the spectra in Figure 7. First, it is quite clear that as the sample temperature is increased above ~120 K some averaging process is occurring. A comparison with the spectra in Figure 4 shows for $[Fe_3O(O_2CCH_3)_6(4\text{-Et-py})_3](4\text{-Et-py})$ that below ~120 K there are distinct high-spin Fe^{II} and Fe^{III} signals. However, above this temperature the characteristics cannot simply be identified as high-spin Fe^{II} and Fe^{III} signals. At 298 K it can be seen that the two doublets are close to each other. The center shift for each of the two doublets (uncorrected for second-order Doppler shift) is plotted vs. temperature in Figure 8. At temperatures above ~100 K an averaging process is evident. This is made clear by the comparison shown in Figure 8 with center shift data for the Fe^{II} ion in $[Cr_2^{III}Fe^{II}O(O_2CCH_3)_6(py)_3](py)$ and data for the Fe^{III} ion in $[Fe_2^{III}Co^{II}O(O_2CCH_3)_6(py)_3](py)$. It is clear from Figure 8 that above ~100 K the *decrease* in the center shift for the single "Fe^{II}" ion in $[Fe_3O(O_2CCH_3)_6(4\text{-Et-py})_3](4\text{-Et-py})$ per increment of temperature is approximately twice the increase in center shift observed for the two "Fe^{III}" ions. This is what would be expected from an averaging process that is occurring rapidly relative to the Mössbauer time scale.

The second observation that can be made of the spectra plotted in Figure 7 is that, even though some averaging process is occurring in the ~100–300 K range, the line widths of the components of the two doublets do *not* change as the temperature is increased. If the averaging process involved simply thermally activating a given triangular complex over a potential energy, then line broadening would be expected and the components of the two doublets would first broaden and then coalesce into one average but broadened doublet which eventually would sharpen into a doublet with "normal" line widths. That is, as the sample temperature is increased the rate of thermal electron transfer would increase, eventually to cross the ^{57}Fe Mössbauer window where the Mössbauer line shapes should be affected. A plausible explanation for why this does not happen will be advanced in the next section.

The third observation that can be made about the spectra in Figure 7 is that the area ratio of "Fe^{III}" to "Fe^{II}" doublets does *not* remain fixed at 2:1 as the sample temperature is increased. Figure 9 shows this ratio plotted as a function of temperature from 6.5 to 298 K. Above ~150 K this area ratio increases gradually to become 3.55:1 at 298 K. The same area ratio is plotted in

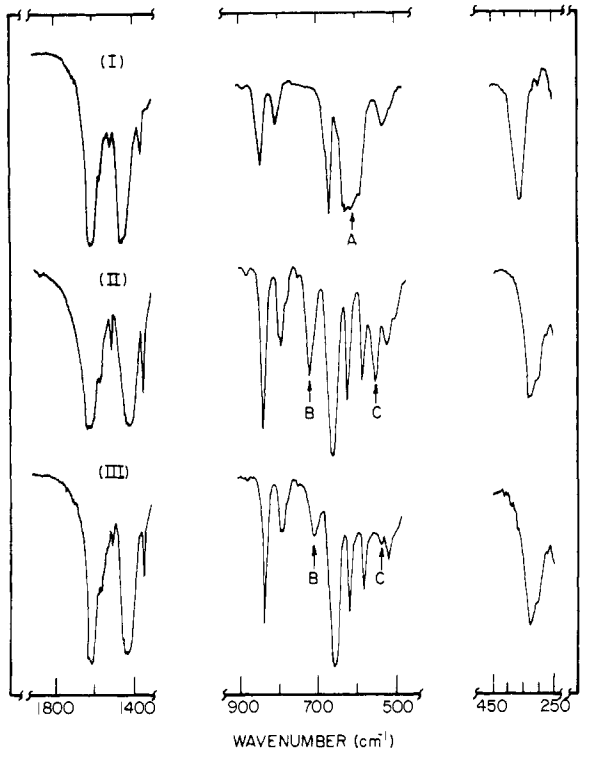

Figure 10. Room-temperature FT-IR spectra of KBr pellets: (I) $[Fe_3^{III}O(O_2CCH_3)_6(4\text{-Et-py})_3]ClO_4$; (II) $[Fe_2^{III}Co^{II}O(O_2CCH_3)_6(4\text{-Et-py})_3](4\text{-Et-py})$; and (III) $[Fe_3O(O_2CCH_3)_6(4\text{-Et-py})_3](4\text{-Et-py})$.

Figure 9 for $[Fe_3O(O_2CCH_3)_6(py)_3]$, a compound that does not show an averaging process at temperatures approaching room temperature. The increase in the ratio to 3.5 at 295 K for the 4-Et-py compound simply means that, compared to the two "Fe^{III}" sites, the recoilless fraction of the one "Fe^{II}" site is becoming less and less as the temperature is increased. This is further evidence that the 4-Et-py ligand bonded to this one "Fe^{II}" ion is changing from statically disordered at low temperature to dynamically disordered at high temperatures. Movement of the disordered ligand between its two positions at a rate that is fast on the Mössbauer time scale could well lead to a reduced recoilless fraction at the one "Fe^{II}" site.

Cannon et al.[21] have examined the IR spectra of the mixed-valence complexes $[Fe_3O(O_2CCH_3)_6L_3]$, where L is H_2O or pyridine. If such a complex has D_{3h} site symmetry and is totally delocalized electronically, then one doubly-degenerate asymmetric Fe_3O stretch would be expected. Cannon et al. have identified such a band near 600 cm^{-1} for the $[Fe_3^{III}O(O_2CCH_3)_6(H_2O)_3]^+$ ion. In the mixed metal complexes of composition $[Fe_2^{III}MO(O_2CCH_3)_6(H_2O)_3]$, where M is Mn^{II}, Co^{II}, or Ni^{II}, they found that the reduction in site symmetry from D_{3h} to C_{2v} lifted the degeneracy of the asymmetric Fe_3O stretch and two bands were seen. They also found that in the case of the mixed-valence complex $[Fe_3O(O_2CCH_3)_6(H_2O)_3]$ the same splitting into two bands is seen for the asymmetric Fe_3O stretching modes. However, the splitting is somewhat smaller in the case of the mixed-valence complex than in the case of the mixed-metal complexes. They interpreted this to mean that the two oxidation states of the iron ions as distinguishable on the infrared time scale in the mixed-valence complex but that "they are not so sharply distinct as if they were pure Fe^{III} and Fe^{II}".

In Figure 10 are given room-temperature IR spectra of KBr pellets of $[Fe_3^{III}O(O_2CCH_3)_6(4\text{-Et-py})_3]ClO_4$, $[Fe_2^{III}Co^{II}O(O_2CCH_3)_6(4\text{-Et-py})_3](4\text{-Et-py})$, and the mixed-valence complex $[Fe_3O(O_2CCH_3)_6(4\text{-Et-py})_3](4\text{-Et-py})$. In each case the bands in three spectral regions are illustrated: the asymmetric and symmetric carboxylate (CO_2) stretching region (~1400–1600 cm^{-1}), the asymmetric M_3O stretching region (~500–700 cm^{-1}), and the metal–oxygen (carboxylate) stretching region (~350 cm^{-1}). As is evident in Figure 10, there are *not* appreciable differences in the CO_2 region for the three complexes. Basically two strong bands are seen in each case. The splitting between the two CO_2 bands is greater for the $Fe_2^{III}Co^{II}O$ complex than for the $Fe_3^{III}O$ complex. The splitting in the CO_2 bands for the mixed-valence complex is intermediate between the values for the other two complexes.

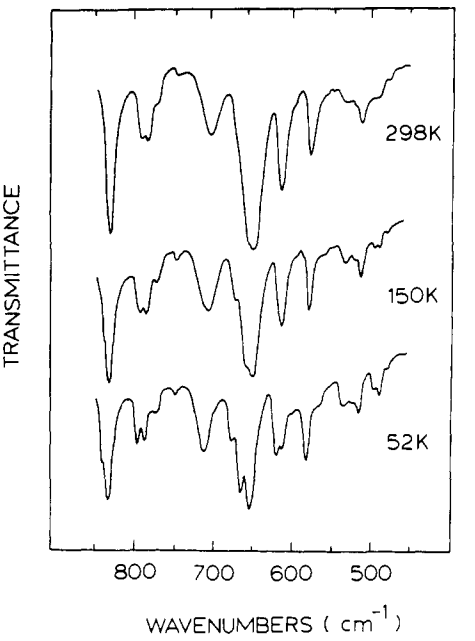

Figure 11. Variable-temperature FT-IR spectrum of the KBr pellet of $[Fe_3O(O_2CCH_3)_6(4\text{-Et-py})_3](4\text{-Et-py})$.

The M_3O asymmetric stretch regions of the IR spectra are most revealing. The $Fe_3^{III}O$ complex shows only one such stretching band which is marked as A in the spectrum. The $Fe_2^{III}Co^{II}O$ complex exhibits two such bands, marked B and C in the spectrum for this complex. It also appears that the mixed-valence complex shows these same two asymmetric M_3O stretching bands. It can be concluded that this mixed-valence complex is localized on the infrared time scale. The rate of intramolecular electron transfer is less than $\sim 10^{12}$ s^{-1}.

Figure 11 shows the temperature dependence of the IR spectrum of the mixed-valence complex. There is very little that happens to the IR spectrum in the Fe_3O stretch region when this complex is cooled to 52 K. Some improved resolution is evident in certain bands, and the Fe_3O stretching bands at 718 and 540 cm^{-1} increase somewhat in intensity relative to other bands.

Valence-Detrapping Modes in the Solid State. In terms of the PKS vibronic model[33] for the electronic structure of mixed-valence complexes it is clear that both the electronic coupling between neighboring metal ions and the level of vibronic coupling will not change appreciably in the series $[Fe_3O(O_2CCH_3)_6(py)_3](solvate)$ as the solvate molecule is changed. Due to the near electronic degeneracy in this triangular mixed-valence complex, it serves as a very sensitive probe of the nature of the solid state. It is our hypothesis that the temperature dependence that is seen in the Mössbauer spectra for several of these mixed-valence Fe_3O acetate complexes is *not* just the result of directly thermally activating complexes to overcome a potential-energy barrier for electron transfer. It is likely that the temperature dependencies that are seen are the manifestation of dynamics of ligands and solvate molecules in the solid state, not directly *intra*molecular electron transfer. The onset of dynamical motion in the solid at a certain temperature modifies the environment about a particular mixed-valence complex. The new environment changes the potential-energy barrier such that intramolecular electron transfer occurs at a considerably faster rate.

The temperature dependence seen in the Mössbauer spectra (Figure 7) for $[Fe_3O(O_2CCH_3)_6(4\text{-Et-py})_3](4\text{-Et-py})$ is probably the result of an order–disorder phase transition. At low temperatures the ordered phase is comprised of a statically and

randomly disordered array of 4-Et-py ligand and solvate molecules. If there was a high level of cooperativity between the Fe_3O complexes throughout the solid, then a first-order phase transition would be experienced, so that as the temperature of the solid is increased suddenly large regions of the statically disordered complexes would become dynamic. The 4-Et-py ligand would be jumping rapidly between its two positions. The information about motion in one disordered 4-Et-py ligand could be conveyed to another Fe_3O complex by dynamic disorder in the solvate molecule. This coupled motion in the solid in essence is a phonon and, if it existed, it would be the valence-detrapping mode in the solid state. Depending on the packing arrangement in the solid, that is, the intermolecular contacts and possibilities for dynamics in parts of the solids, certain of these mixed-valence Fe_3O complexes will show a temperature dependence in their properties. One can speculate that no intramolecular electron transfer is evident in the variable-temperature Mössbauer data for $[Fe_3O(O_2CCH_3)_6(py)_3]$ because the lattice in this compound is packed so tightly that pronounced intermolecular contacts prevent any motion of any parts of this solid.

The presence of phase transitions has already been firmly established for two of these mixed-valence Fe_3O complexes. As we report in another paper,[34] variable-temperature heat capacity results (12–300 K) clearly indicate the presence of two phase transitions for $[Fe_3O(O_2CCH_3)_6(py)_3](py)$ in the solid state.

There are two final points that sould be addressed concerning the data presented above. The first point is the rather large temperature ranges over which the transformations from localized to delocalized occur, as indicated by the Mössbauer spectra. In Figure 7, or more particularly Figure 8, it can be concluded that it takes 100–150 degrees for the transformation from localized to delocalized to occur for the 4-Et-py complex. For a phase transition with any degree of cooperativity, domains of a minority phase nucleate and grow in the presence of the majority phase. It has been shown that defect concentration in a crystallite can make a cooperative phase transition very gradual in its development. Defects in a crystal may come in the form of vacancies, isolated impurities, dislocations, grain boundaries, or surface imperfections.

The second point is the matter of no line broadening seen in the Mössbauer spectra even though there is some process of averaging present. It must be admitted that with complicated spectral data as shown in Figure 2 for $[Fe_3O(O_2CCH_3)_6(py)_3](py)$, where at some intermediate temperatures there are at least five peaks visible, it is difficult to decide whether or not line broadening is present. However, the spectra for the 4-Et-py complex do *not* show any evidence of line broadening. We have prepared and characterized several other mixed-valence Fe_3O complexes that show temperature-dependent spectra, but no line broadening. Furthermore, four different substituted mixed-valence biferrocenium triiodide salts have now been characterized that also exhibit a localized to delocalized transformation in their Mössbauer spectra, again clearly with no line broadening.[35]

The phonon mode that leads to the phase transition in these complexes is obviously occurring at a frequency greatly in excess of the Mössbauer time scale. At low temperatures the environment about each mixed-valence Fe_3O complex is static. The static environment is asymmetrically disposed relative to the three iron ions in one triangular complex. The *intra*molecular electron transfer is relatively slow because the potential-energy barrier is increased due to this asymmetric environment. As the temperature of the sample is increased, the "valence-detrapping" phonon mode(s) becomes activated. Small *minority* domains form where all the molecules have a dynamic 4-Et-py ligand. At certain temperatures many of these small minority domains will revert to being part of the majority domain where the ligands are static. At any temperature there is a critical size that a minority domain has to achieve in order to continue to grow. If the rate at which a given Fe_3O complex moves back and forth between majority and minority domains is always fast compared to the Mössbauer time scale, if the motion of 4-Et-py ligand is also fast in the minority domain, and finally if the *intra*molecular electron transfer is fast in the minority dynamic domain, then the type of Mössbauer behavior that is being seen would be expected. The low-temperature Fe^{II} and Fe^{III} doublets would just move together to become a single average doublet. There would be no line broadening. Finally, if the frequency of the above lattice dynamics and electron transfer are less than $\sim 7.5 \times 10^{12}$ s^{-1}, then the complex would appear to be localized in terms of IR bands above 250 cm^{-1}.

Conclusions and Comments

Three basic observations have been made about *intra*molecular electron transfer in the *solid state* for mixed-valence $[Fe_3O(O_2CCH_3)_6L_3](solvate)$ complexes. First, the rate of electron transfer is dramatically affected by changing the solvate molecule. Second, in several cases no line broadening is seen in the separate Mössbauer signals as they move together at higher temperature to become an average signal. Third, the distances in the mixed-valence Fe_3O complex change appreciably with a change in sample temperature. The Fe_3 triangle becomes more symmetric at higher temperature. A transformation in the solid state involving a conversion from statically disordered at low temperatures to dynamically disordered at high temperatures is involved. Ligands and/or solvate molecules are becoming dynamic at high temperatures.

It needs only briefly to be mentioned here that observations similar to those noted in this work are being made in other areas of research. The effect of changes in solvate molecules upon spin-crossover complexes has been noted.[36] It would be anticipated that not only bulk properties reflecting the amounts of low- and high-spin complexes present would respond to changes in the solvate molecule but the rate of spin-crossover interconversion in the solid state should reflect the nature of the solvate molecules.[37] Order–disorder transformations in the solvate molecules have been noted for spin-crossover complexes. Other electronically labile complexes such as Jahn–Teller distorted complexes should have similar sensitivities. It has also been noted that the nature of the order–disorder in the ClO_4^- counterion affects the conductivity of stacked organic molecules.[38]

Acknowledgment. We thank the National Institutes of Health for support of the work at the University of Illinois through Grant HL13652 to D.N.H. and the Robert A. Welch Foundation for support of the work at the University of Texas at Austin through Grant F-233 to R.E.D.

Supplementary Material Available: Tables of observed and calculated structure factor amplitudes, fractional crystallographic coordinates, thermal parameters, full listings of bond lengths and angles, selected torsion angles, and selected least-squares planes for both structure determinations of $[Fe_3O(O_2CCH_3)_6(4\text{-Et-py})_3](4\text{-Et-py})$ (59 pages). Ordering information is given on any current masthead page.

(33) Wong, K. Y.; Schatz, P. N. *Prog. Inorg. Chem.* **1981**, *28*, 369.
(34) Oh, S. M.; Ksambara, T.; Hendrickson, D. N.; Sorai, M.; Kaji, K.; Woehler, S. E.; Wittebort, R. J. *J. Am. Chem. Soc.*, in press.
(35) Dong, T.-Y.; Hendrickson, D. N.; Iwai, K.; Cohn, M. J.; Geib, S. J.; Rheingold, A. L.; Sano, H.; Motoyama, I.; Nakashima, S. *J. Am. Chem. Soc.*, preceding paper in this issue.
(36) (a) Gütlich, P. *Struct. Bonding (Berlin)* **1981**, *44*, 83. (b) König, E.; Ritter, G.; Kulshreshtha, S. K. *Chem. Rev.* **1985**, *85*, 219–234. (c) Rao, C. N. R. *Int. Rev. Phys.* Chem. **1985**, *4*, 19–38.
(37) Federer, W. D.; Hendrickson, D. N. *Inorg. Chem.* **1984**, *23*, 3861, 3870.
(38) Moret, R.; Pouget, J. P.; Comes, R.; Bechgaard, K. *Phys. Rev. Lett.* **1982**, *49*, 1008.